IEEE Access
Multidisciplinary | Rapid Review | Open Access Journal

Received September 19, 2020, accepted October 3, 2020, date of publication October 23, 2020, date of current version November 12, 2020.

Digital Object Identifier 10.1109/ACCESS.2020.3033284

Beam-Scanning Antenna Based on Near-Electric Field Phase Transformation and Refraction of Electromagnetic Wave Through Dielectric Structures

MUHAMMAD U. AFZAL[1], (Senior Member, IEEE), LADISLAU MATEKOVITS[2,3,5], (Senior Member, IEEE), KARU P. ESSELLE[1], (Fellow, IEEE), AND ALI LALBAKHSH[4], (Member, IEEE)

[1]School of Electrical and Data Engineering, University of Technology Sydney, Ultimo, NSW 2007, Australia
[2]Department di Elettronica e Telecomunicazioni, Politecnico di Torino, 10129 Torino, Italy
[3]Faculty of Electronics and Telecommunications, Politehnica University Timisoara, 300223 Timisoara, Romania
[4]School of Engineering, Macquarie University, North Ryde, NSW 2109, Australia
[5]Istituto di Elettronica e di Ingegneria dell'Informazione e delle Telecomunicazioni, National Research Council, 10129 Turin, Italy

Corresponding author: Muhammad U. Afzal (muhammad.u.afzal@ieee.org)

We acknowledge the support of University of Technology Sydney and Australian Government under the Australian Research Council Discovery Scheme.

ABSTRACT An elegant combination of electric near-field phase transformation technique and electromagnetic-wave refraction, implemented through a pair of 3D printed dielectric structures, has been used to demonstrate a Ka-band beam-scanning antenna system. The system comprises a resonant-cavity antenna (RCA), which is used as a base antenna, a stepped dielectric (SD), and a dielectric wedge (DW). The SD is suspended above RCA in the near-field region to focus its broadside beam at an offset angle of 20°. The DW is placed above the SD and its two opening angles are selected such that the offset-angle focused beam tilts further and moves back to the broadside when the DW is co- and counter-aligned with the SD, respectively. The total height of the antenna system is $8.1\lambda_0$, where λ_0 is the free-space wavelength at the operating frequency of 30 GHz. The total cost of the material used for printing the two dielectric structures in prototyping is only 6 USD. It has been demonstrated through measurements of the prototype that by rotating the DW around its own axis, the antenna beam can be scanned in both azimuth and elevation planes. The measured results indicate that antenna beam can effectively be scanned to any arbitrary angular position within a conical region having an apex angle of 68°, while maintaining peak-gain value within the 3 dB limit of the maximum gain of 16 dBi.

INDEX TERMS Beam-scanning, beam-steering, low-cost antennas, phase-shifting structures, rapid prototyping, resonant-cavity antenna, 3D printing.

I. INTRODUCTION

Beam-scanning antenna is among the most widely researched topics in the field of wireless communication due to a range of upcoming applications involving moving platforms such as low-earth-orbit (LEO) satellites and CubeSats [1]–[3]. A noteworthy application is precision farming, which allows farmers to maximize the yield of their crops by having access to consistent and accurate sensors' data from remote farms via CubeSats [4]. CubeSats operate in non-geosynchronous orbits and pass above same geographical locations several times in a day. These satellites collect data through a dedicated uplink channel from a remote location, which is then downloaded at a data center for analysis through a downlink [5]–[9]. Since satellites are non-stationary, there is a small window of time available for the upload and download communication links to transfer the data to and from the CubeSats, respectively, before it moves out of the coverage of ground station antenna [10].

A network of ground stations having multiple low-cost beam-scanning antennas can be used to continuously track CubeSats over the horizon and increase the connectivity time for data transfer [11]. A major limitation of this model is that the beam scanning is inherently an expensive antenna

The associate editor coordinating the review of this manuscript and approving it for publication was Yasar Amin.

technology that requires sophisticated electronic components and manufacturing facilities. It is for these reasons that beam-scanning antennas are mostly used in defense and only in high-end civilian applications such as in-flight connectivity. To enhance the application spectrum of beam-scanning antennas, this paper proposes a novel solution that is developed using a combination of near-field phase transformation theory [12], [13] using stepped dielectric (SD) and refraction of electromagnetic (EM) wave through a dielectric wedge (DW). The antenna system comprises a resonant-cavity antenna (RCA) and a pair of SD and DW. The SD is designed to realize near-field phase transformation and effectively tilt the RCA beam. The DW is optimally designed using optical ray tracing to tilt the beam further and move to move the beam in the broadside direction when DW is co and counter aligned with the SD, respectively. The SD and DW are both 3D printed using a readily available polylactide (PLA) plastic and a moderate 3D printer. The SD and DW are placed above the RCA and are physically rotated, independently and synchronously, around the center of the aperture to scan the antenna beam in a 2D angular region. This method of beam-scanning is continuous, unlike switched beam type antenna arrays [14], [15]. However, the beam-scanning speed of the proposed method is limited by the mechanical rotation of the dielectric structures and slower than the electronically switched arrays. The proposed design is novel when compared with those reported in the literature. In comparison to the beam-steering antenna that uses two dielectric wedges, with matching layers, and a tall conical horn feed [16], [17], the proposed design uses much shorter RCA and thus have a reduced height profile. The dielectric structures used in the proposed antenna can be developed using commonly available 3D printer and are extremely cheaper when compared with multilayered printed phase-shifting surfaces and printed metasurfaces [12], [18]. The multilayer printed circuit board not only needs expensive multiple dielectric laminates but also requires specialized manufacturing facility for bonding several layers into a single surface. The proposed design thus greatly reduces the cost and pave the way for the development of low-cost antennas. The maximum height of the proposed design is only $8.4\lambda_0$, which is 40% less than the maximum height of the most closely related and recently reported millimeter-wave beam scanning antenna [19]. Furthermore, the fabrication cost of the parts used in the proposed design is extremely low than that of the two stepped dielectrics developed using traditional subtractive manufacturing technique.

The rest of the paper is organised such that first the physics and working principle of the antenna is explained in Section II. The procedure to design a stepped dielectric (SD) is given in Section III. A design example is discussed in Section IV along with the ray-tracing used to optimise opening angles of the DW. Measured results of a fabricated prototype are discussed in Section V and paper is concluded at the end.

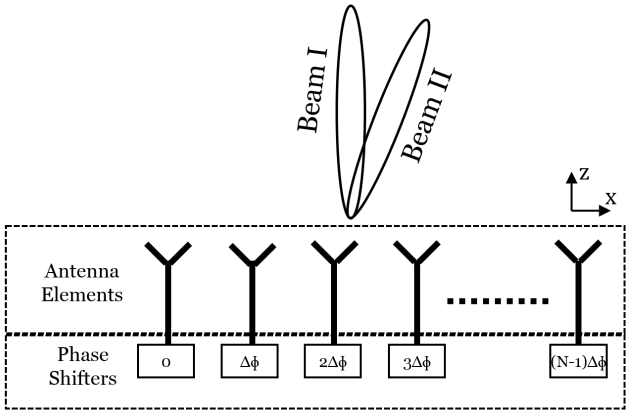

FIGURE 1. A 1D array of N identical radiating antenna elements. Each element of the array has a phase shifter attached at the input of the antenna.

II. PHYSICS OF BEAM-SCANNING METHOD

To understand the physics of the proposed beam-scanning antenna, the principle of phased arrays and the propagation-phase delay of the electric field through a dielectric is first briefly explained. Consider a closely packed 1D array of 'N' antenna elements, as shown in Fig. 1. In this array, each antenna is individually fed from a separate source, and additionally, there is a phase shifter to control the phase of the RF signal. If all antenna elements in the array are fed synchronously, so that there is no relative phase difference, then the array beam peak will be along +z-axis (Beam I). If the phase shifts are adjusted such that there is a increasing phase delay along the array axis (+x-axis), then the beam peak tilts at an angle away from the +z-axis (Beam II). In phased arrays, the phase delay is achieved using external radio frequency (RF) phase shifters that are inserted in the RF path before the antenna elements.

A different approach to effectively tilt the array beam by introducing the phase delay through a free-standing near-field phase-transforming structure is used here [20]. These phase-transforming structures have spatially distributed phase-shifting cells to locally transform the phase of the incoming electric field into a desired phase of the outgoing field. This strategy of manipulating the phase of the radiated field has some advantages in terms of cost and power losses when compared with phase shifters in arrays.

One type of free-standing phase-transforming structure is made from dielectric materials [20], [21]. It is well-known that the wavelength of electric field propagating inside a dielectric is less than that in the free space, which is expressed as $\lambda_g = \lambda_0/\sqrt{\varepsilon_r}$, where λ_0 is the free space wavelength and ε_r is the relative permittivity of the dielectric. A plane wave propagating through an infinitely extended dielectric material experiences a phase delay, which is directly proportional to the relative permittivity and length of the dielectric. The phase-delay through a dielectric can be varied either using different lengths of a same dielectric material or using different dielectric materials of a fixed length. This work focuses

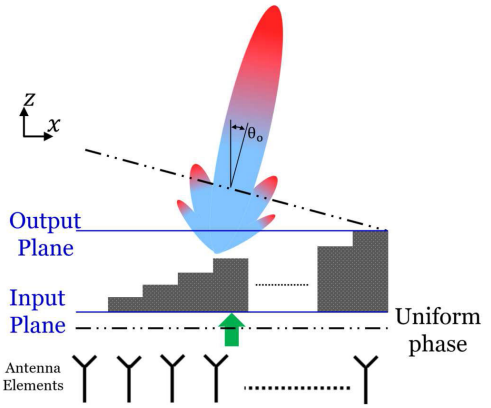

FIGURE 2. A stepped dielectric used to create a linear phase progression and thus tilts the beam at an offset angle.

on using variation in the length of a fixed dielectric material to achieve the desired phase delay profile with an SD.

Consider a cross-section view of an SD that placed above an array as shown in Fig. 2. The figure depicts the propagation of electric field through an SD that is made of several dielectric section of different heights. The electric field, propagating along +z-axis, at the input of the SD has uniform phase distribution represented by a parallel line. The electric field passes through each dielectric section of the SD. Each section has a different length and thus provide a different phase delay between two parallel planes marked at the input and output of the SD. The heights of sections in the SD can be adjusted to transform a uniform phase at the input plane into a linearly decreasing phase at the output plane to effectively tilt the beam by an angle $\theta_\circ$. The heights of the dielectric sections in a SD are calculated with array theory, which will be discussed in the latter sections.

A single SD can tilt the array beam at a fixed offset angle away from the broadside direction. The beam direction can be dynamically changed using an optical beam-scanning concept of Risley Prisms. In this optical-scanning method, two prisms are placed in front of an optical source where each prism tilts the optical beam away from the normal direction [22]. The prisms are placed in the far-field region of the optical source and while keeping the source fixed the prisms are rotated synchronously and independently to dynamically scan the optical beam in a large conical region. The azimuth and elevation angles of the beam depend on the orientation of the two prisms.

Similar to Risely Prisms, the proposed antenna uses a second beam-tilting structure made of DW, which is pictorially depicted in Fig. 3. The DW, unlike SD, is designed using ray-tracing method. The two opening angles of the DW are calculated by tracing rays from the input edge of the DW to the output edge in two extreme scenarios depicted in Fig. 3. For the sake of clarity, from hereafter the orientation angles of SD and DW, measured in the counter-clockwise direction from +x-axis, will be represented by symbols ψ_1 and ψ_2, respectively.

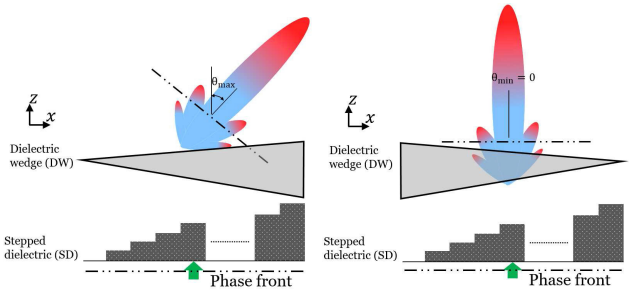

FIGURE 3. A pictorial depiction of stepped dielectric (SD) and dielectric wedge (DW) with beam directions.

In the picture on the left, the DW is aligned with the SD or $\psi_1 = \psi_2 = 0°$, so that the broadside beam from the a array is tilted to a maximum angle in the elevation plane. In the second case, on the right side, the DW is physically pointing in the direction opposite to the SD or $\psi_1 = 0°$ & $\psi_2 = 180°$, and the beam is moved in the broadside. The beam can be moved to any intermediate elevation angle using an appropriate combination of ψ_1 and ψ_2. A set of equations can be used to find optimal opening angles of DW such that these two extreme cases are satisfied when the SD and DW are co and counter aligned. Further details on the designing of SD and DW are in the following sections.

III. STEPPED DIELECTRIC (SD)

An SD can be designed for any large aperture antenna or an array to transform is near-electric field phase distribution. Therefore, a generic design process is explained for a hypothetical 'base' antenna. First, a plane is defined on the base antenna at a distance between $\lambda_0/4$ to λ_0, where λ_0 is the free-space wavelength at the operating frequency. In this plane, a finite area that is typically equal to the aperture area of the base antenna is considered for phase transformation. The area is then divided into a 2D grid of cells having N rows and N columns, as shown in Fig. 4. The side length (d) of cells is set around $\lambda_0/3$, which is fixed based on the outcomes of earlier investigations on near-field phase correction [20]. Each cell is identified by an ordered pair (m,n) where 'm' is the row number starting from the bottom of the grid, and 'n' is the cell number starting from the left of the grid. The total size of the area, represented here by S, is sometimes slightly adjusted to ensure that it is perfectly discretized into cells of length d.

Each cell of the grid is treated as an element of a 2D array and phase delay for each cell is calculated using array theory. The array theory states that to tilt a beam by an angle $\theta_\circ$, in an array that has antenna elements with center-to-center spacing of d and operating at wavelength λ_0, the progressive increase in phase delay or δ is:

$$\delta = \frac{2\pi}{\lambda_0} d \sin(\theta_\circ). \tag{1}$$

The phase delay for any cell (m, n) of the grid can be calculated with reference to cell (1,1) using $\Delta\phi(m, n) = (n-1)\delta$, – it is to be noted here that all rows within a column have same phase delay.

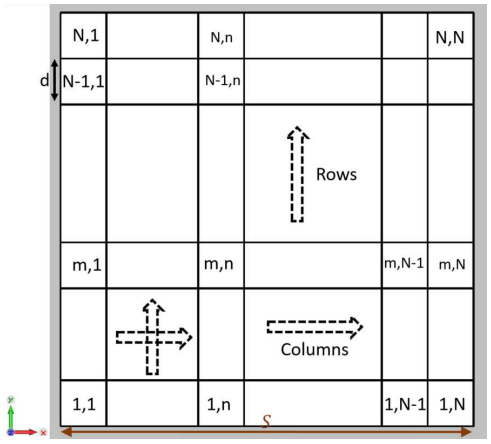

FIGURE 4. Discretized plane on the aperture of a base antenna with 2D array of identical cells.

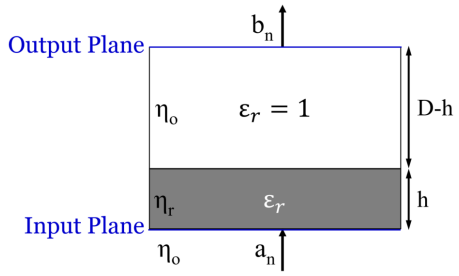

FIGURE 5. Phase delay between two parallel planes occupied by a dielectric and air regions of fixed heights.

The SD is designed by filling the aperture grid with dielectric sections of appropriate heights. To find appropriate heights of dielectric section, the propagation of the electric field through a dielectric is briefly explained using Fig. 5. The figure depicts a dielectric section with relative permittivity ε_r and height h and an air section with height $D - h$. The total phase delay experienced by propagating electric field between these two planes is the sum of phase delay in dielectric and phase delay in the air region, analytical expressed by a simplified equation [23]:

$$\phi_d(\varepsilon_r, h) = \angle\left(\cos(k_d h) + j\sin(k_d h)\left(\frac{1+\varepsilon_r}{2\sqrt{\varepsilon_r}}\right)\right) + k_0(D-h). \tag{2}$$

The equation reveals that for a dielectric with fixed permittivity and increasing h, the first term increases and the second term linearly decreases. The minimum value of ϕ_d is $k_0 D$, occurs when $h = 0$. Although the phase delay from the second term decreases with the increase in h but the overall value of the ϕ_d increases because the increases in the first term is more than the decrease in the second term. Hence, the ϕ_d can be normalized with its minimum value, which is $k_0 D$. The normalized phase delay is given as:

$$\phi_{d(nor)}(\varepsilon_r, h) = \angle\left(\cos(k_d h) + j\sin(k_d h)\left(\frac{1+\varepsilon_r}{2\sqrt{\varepsilon_r}}\right)\right) - k_0 h. \tag{3}$$

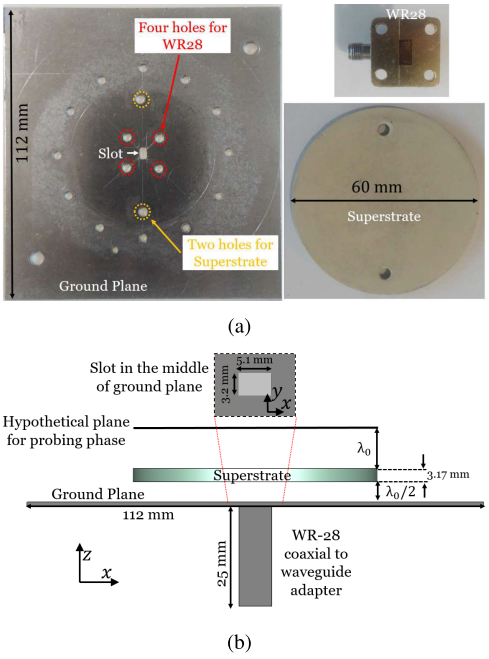

FIGURE 6. (a) Actual photographs of the ground plane, superstrate, and the waveguide adapter used in RCA prototype and (b) A side view the 3D RCA model built for simulations in CST MWS along with key dimensions.

The $\phi_{d(nor)}$ is used to calculated appropriate h for fixed ε_r and required $\phi(m, n)$ using the procedure explained for dielectric phase correction in [20].

IV. DESIGN EXAMPLE

To demonstrate the working principle of the proposed hybrid solution, an antenna system is designed at the operating frequency of 30 GHz using resonant-cavity antenna (RCA) as the base antenna. The three elements of the system are discussed in following three subsections.

A. RESONANT-CAVITY ANTENNA

A classical RCA for its simple feeding arrangement and low height profile was used as a base antenna for the beam-scanning system. RCAs have been extensively investigated in the last decade and also being referred to as electromagnetic band-gap resonator antennas, Fabry-Perot antennas, or partially reflecting surface antennas [24]–[27]. A classical RCA comprises a primary feed, which can be a microstrip patch antenna [20], [28] or a slot antenna [29], [30], backed by an extended ground plane and a partially reflecting printed or unprinted superstrate. The superstrate is suspended at a half-wavelength spacing from the ground plane. The ground and the superstrate form a cavity that resonates at the operating frequency.

A slot antenna was used as the RCA feed here, which was made from a WR-28 [31] coaxial to waveguide adapter and 1 mm thick square aluminum plate. The plate side length was 112 mm. A 3.17 mm thick circular disk of Rogers TMM4 dielectric ($\varepsilon_r = 4.5$) having a physical diameter of 60 mm (or $6\lambda_0$) was used as a superstrate. Actual photographs

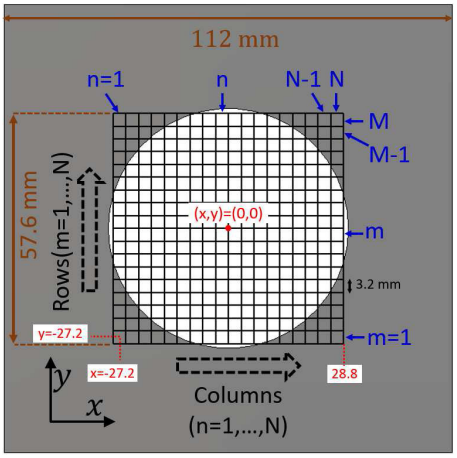

FIGURE 7. Two-dimensional grid of the horizontal and vertical cells, created to discretize the RCA aperture. The electric field radiated by the RCA is probed at the center of each cell using near-field data predicted through full-wave simulations.

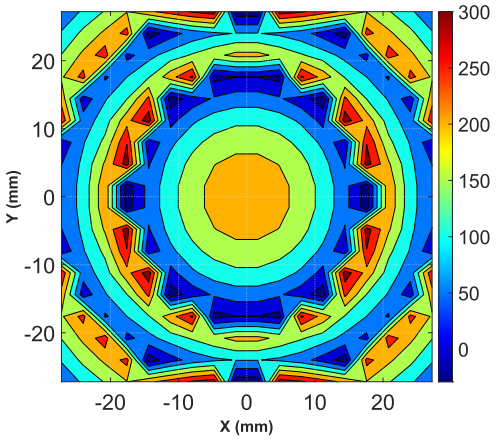

FIGURE 8. Phase distribution of the dominant electric-field component E_y in a plane above RCA.

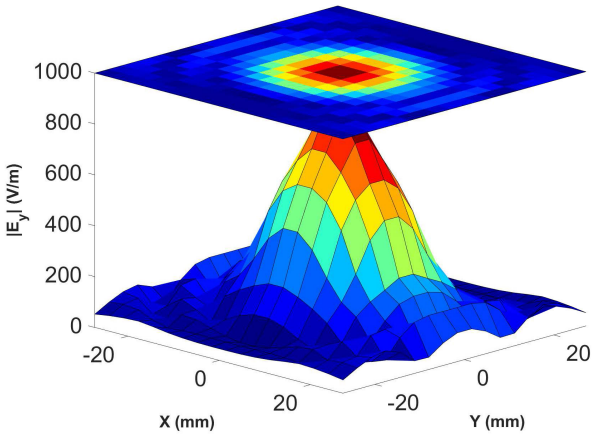

FIGURE 9. Magnitude of the dominant electric-field component ($|E_y|$) radiated by the RCA.

of the ground plane, WR-28 coaxial to waveguide adapter, and the superstrate are shown in Fig. 6(a). It is to be mentioned here that the photographs of WR-28 and the superstrate are enlarged for clarification and are not on the same scale as that of the ground plane photograph. The ground plane has a rectangular slot at the center for excitation and several holes to screw WR-28 coaxial to waveguide adapter and superstrate for prototyping.

The 3D model of the RCA was created and simulated with a time-domain solver in CST Microwave Studio, which is pictorially shown in Fig. 6(b). The superstrate disk is suspended at a spacing of 5 mm (or $\lambda_0/2$) from the ground plane. The size of the slot in the ground plane was optimized to a 5.1 mm $\times$ 3.2 mm to improve RCA impedance matching. At the operating frequency, the RCA had a beam peak the broadside, and maximum directivity was around 15 dBi.

B. SD DESIGN

The SD was designed for the RCA following the procedure discussed previously. First, a square area with side length ($S = 57.6$ mm) was defined at a one wavelength spacing (or 10 mm) exactly above the superstrate in a hypothetical plane. The plane was divided into a symmetric 2D grid of square cells having 18 rows and 18 columns or $N = 18$, as shown in Fig. 7. Each cell of the grid has a width and length $d = 3.2$ mm. The reference cell (m,n)=(1,1) is centred at (x_n, y_m)=$(-27.2, -27.2)$ mm with reference to the absolute center of the RCA. The magnitude and phase of the dominant near-electric field component (E_y) were probed at the center of cells (x_n, y_m) in the 2D grid, using near-field data obtained through RCA full-wave simulations. The magnitude and normalized phase are mapped on the aperture grid in Fig. 8 and Fig. 9, respectively. For mathematical convenience, we denoted the aperture grid phase of the RCA electric field by $\phi_{in}(m, n)$. The maximum phase variation on the aperture is more than 360° and the electric field is mainly concentrated at the center of the aperture with negligible magnitude towards edges. The phase of the electric field was not uniform and was corrected in the SD design. The phase correction, however, was performed only in the limited aperture due to the fact that the electric field strength reduces towards edges. The maximum magnitude of the electric field at the center of the aperture is 852 V/m. For phase correction, a limited region of the aperture where the magnitude of the electric field is above 150 V/m was considered. This region is made of central ten rows and ten columns of the grid in Fig. 7, i.e. between $m = n = 5$ and $m = n = 18$. The phase delay required for the correction, referred to as $\phi_c(m, n)$ hereafter, in this reduced region was included in SD design.

In principle, $\phi_c(m, n)$ is a positive 2D distribution, which when subtractive from $\phi_{in}(m, n)$ gives a constant value. The $\phi_c(m, n)$ is thus chosen same as $\phi_{in}(m, n)$ in the central region and was assumed 0^o outside that region. A detailed step-by-step procedure of near-field phase correction is reported with a design example in [20] and is not repeated here for brevity. To steer beam at an angle of 20° (or for $\theta_\circ = 20°$) a second 2D phase delay is needed, which is denoted by $\phi_s(m, n)$. The $\phi_s(m, n)$ is generated using the progressive phase delay

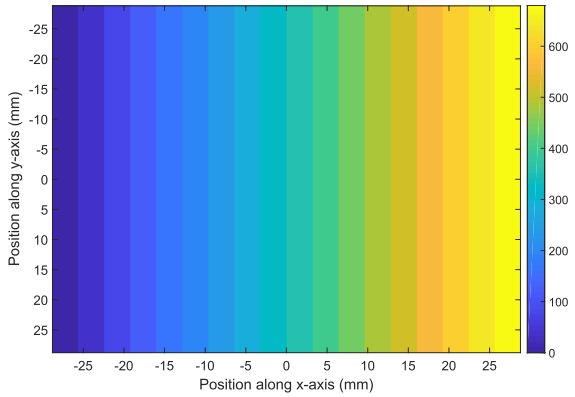

FIGURE 10. Transmission phase delay required to the tilt beam by 20^o.

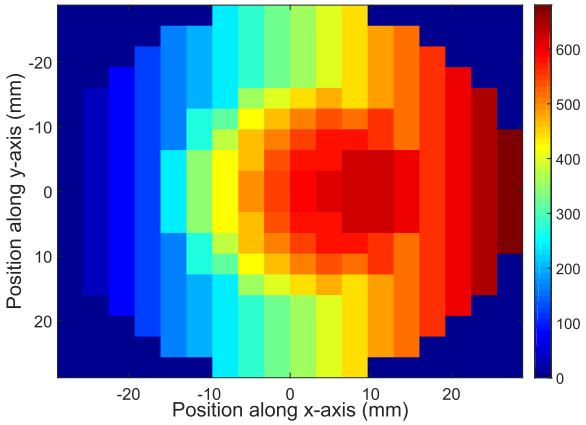

FIGURE 11. Net transmission phase delay of the SD obtained by adding correction and steering phase delays.

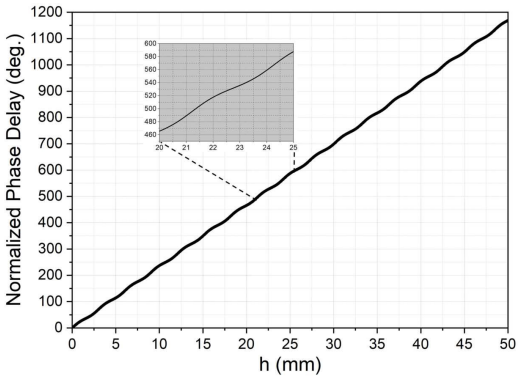

FIGURE 12. Normalized phase delay between two parallel planes separated by a fixed distance $D = 50$ mm. The space between the two planes is filled with dielectric material of $\varepsilon_r = 2.72$ and varying height h.

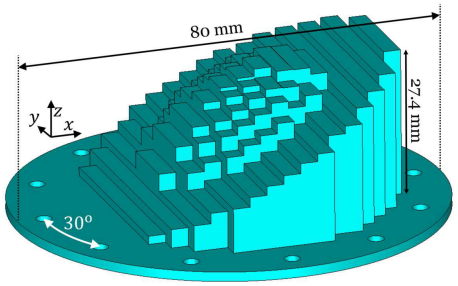

FIGURE 13. Perspective view of the SD 3D model. A ring of small holes at outer edges is for the screws to fix SD above RCA with cylindrical spacers.

obtained through equation (1). In the equation, the center-to-center spacing or $d = 3.2$ mm, which is the size of 2D grid cells. At the operating frequency of 30 GHz and for $\theta_\circ = 20°$, the progressive phase delay is 40° or $\delta = 40°$. Unlike $\phi_c(m, n)$, the $\phi_s(m, n)$ was generated for the whole 2D grid. All rows in the the left most column of the grid (n=1) was assigned a phase delay of 0° or $\phi_s(m, 1) = 0°$. All the subsequent columns have a incremental phase-delay value of 40° or $\phi_{out}(m, n) = (n - 1) \times 40$. The $\phi_s(m, n)$ for a square aperture is mapped using colored pixels in Fig. 10.

Since the SD simultaneously introduces correction and steering phase delays to focus and tilt the RCA beam, its net-phase delay denoted by $\phi_d(m, n)$ was calculated using:

$$\phi_d(m, n) = \phi_c(m, n) + \phi_s(m, n) \tag{4}$$

The $\phi_d(m, n)$ is pictorially represented by color map in Fig. 11 and is used to directly design the SD.

For this purpose, first, we use (3) to calculate the normalized phase delay through a dielectric shown in Fig. 5. The permittivity of the dielectric is fixed to 2.72 or $\varepsilon_r = 2.72$, which is the relative permittivity of the 3D printable plastic material. The dielectric height or h is varied between 0 mm to 50 mm and the $\phi_{d(nor)}$ is calculated, which is plotted in Fig. 12. It is worth emphasizing here that, as previously reported, the minimum transmission magnitude through a dielectric depends on its relative permittivity [28]. A dielectric material with higher relative permittivity has a lower minimum magnitude of transmission, which can create areas of low transmission in the SD. Typically, near-field surfaces and structures are designed to have a transmission magnitude of more than −1 dB. More details on the effects of the relative permittivity of dielectric and their transmission characteristics are available in [23], [28], and are not included here for brevity.

The $\phi_d(m, n)$ is matched with the $\phi_{d(nor)}$ to estimate dielectric heights or $h(m, n)$ in each cell of the 2D grid. Since the RCA has a circular aperture, cells of the grid that are inside the overlapping circular aperture are considered while those at corners are ignored. The 3D model of the SD is developed using the $h(m, n)$, as shown in Fig. 13. It is to be mentioned here that the shape of the SD corresponds to the pattern in the required net phase-delay profile or $\phi_d(m, n)$. For prototyping, a circular disk of height 1.8 mm is created at the base of the SD. The disk additionally has a ring of holes at outer edges with an angular spacing 30°, to fix and rotate the SD above the RCA.

The RCA with the SD, as shown in Fig. 14, was simulated with the time-domain solver of CST Microwave Studio. The SD is placed over RCA at a spacing of $1\lambda_0$ by fixing it with plastic screws on top of four 8 mm diameter spacers. The height of the SD at the thickest side is approximately $3\lambda_0$. The relatively large thickness of the dielectric structure leads to the leakage of the electric field in the sidewalls of the SD.

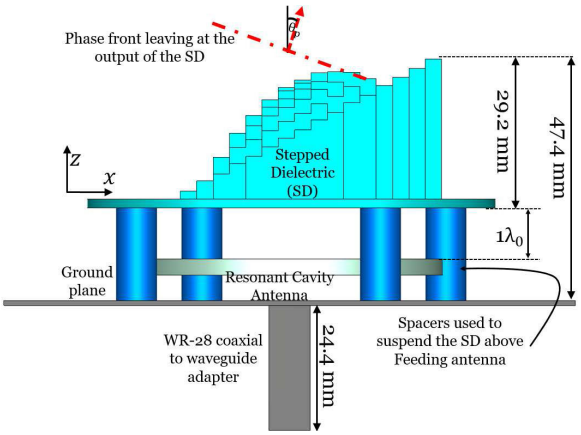

FIGURE 14. Side view of the RCA with SD; four blue colored spacers are not part of antenna design and are used to suspend the SD on the RCA. The phase of electric field at the output of SD is marked with a red dashed line.

This results in far-field pattern distortion and to address this issue, we have used a ring of absorber around the SD to absorb the lateral propagation of the electric field. An improvement in the quality of the radiation pattern is observed at the cost of reducing antenna efficiency and gain. It is to be noted here that SD can be rotated around the antenna axis to scan the azimuth plane while keeping the elevation angle fixed at 20^o as explained with graded-dielectrics in [32].

C. DW DESIGN

To dynamically scan the antenna beam, as explained earlier, a second structure DW is designed and placed over SD. The two opening angles θ_1 and θ_2 of the DW are optimized for the desired system performance. The DW is designed by tracing rays in two different orientation cases of the DW as shown in Fig. 15. The first case is when the thicker part or the DW is pointing along the same direction as that of the phase-progression axis of the SD or $\psi_2 = 0°$. The second case is when the thicker part of the wedge is pointing opposite to the phase progression axis or $\psi_2 = 0°$. In the former case, the antenna beam will be tilted further in the elevation while in the latter the beam moves in the broadside direction.

A system of equations is developed by analysing the two aforementioned configurations for a fixed phase front propagating out of the SD. The two equations give an analytical relationship between the the two output angles as a function of the input angels and the two opening angles of the DW, given as:

$$\theta_{\min} = \sin^{-1}(\sqrt{\varepsilon_r}\sin(\sin^{-1}(\frac{1}{\sqrt{\varepsilon_r}}\sin(\theta_1+\theta_p)) - \theta_1 - \theta_2)) \tag{5}$$

$$\theta_{\max} = \sin^{-1}(\sqrt{\varepsilon_r}\sin(\theta_2+\theta_p)) \tag{6}$$

where θ_p is the propagation angle of the phase front with reference to the normal of the antenna system. To simplify the design, the first opening angle of the wedge or θ_1 is set equal to the beam tilt angle introduced by the SD or $\theta_1 = \theta_p = 20°$. This is to ensure that the phase front propagating out of the SD is perfectly aligned to the input surface of the DW, when the DW is co-aligned with the SD. The θ_{max} and θ_{min} are then calculated for several values of θ_2. For $\theta_2 = 7.8°$, the θ_{min} is 0° or beam is in the broadside direction and $\theta_{max} = 42°$ or the beam is maximally defected in the elevation plane. The opening angles of 20° and 7.8° are used at the input and output faces of the wedge, respectively, to develop 3D model of the DW. The aperture size of the DW is the same as that of the SD with a circular face, as shown in Fig. 16. A 3D model of the antenna system comprising of RCA and a stacked pair of SD and DW are simulated together to verify the beam-scanning principle. A perspective view of the antenna system modeled and used with full-wave EM simulations is shown in Fig. 17. The two additional plastic spacers shown in the figure are for mechanical stability and to fix the DW above SD. These spacers are not part of EM design but are essential for prototyping and measurements.

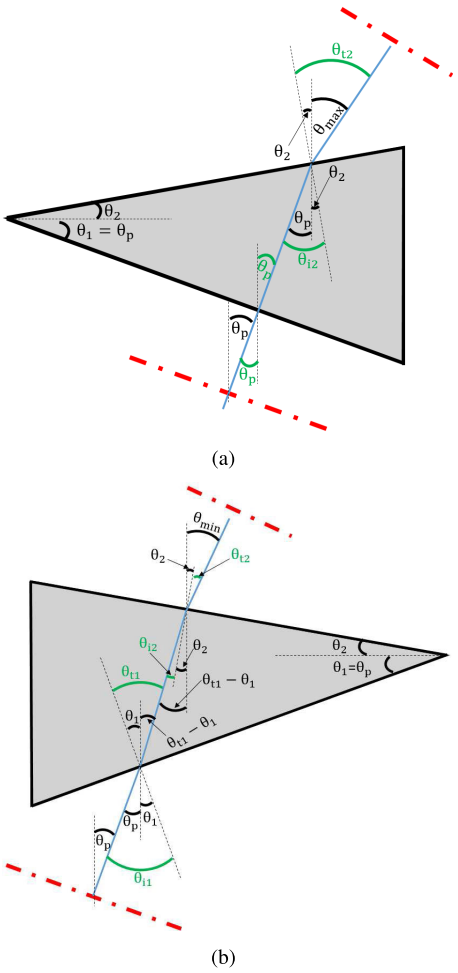

FIGURE 15. Cross-section views of DW for (a) Maximum, and (b) Minimum beam tilt angles along with rays traced (blue color) to calculate the directional of incoming and outgoing waves.

V. RESULTS

The performance of the antenna system was validated by building and measuring a physical prototype. A photograph of the assembled RCA is shown in Fig. 18. The SD and

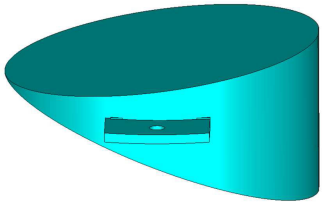

FIGURE 16. A perspective view of the dielectric wedge (DW). Two wing-type supports (one hidden in this view) on opposite sides are introduced for fixing DW in the antenna system and are not part of EM design.

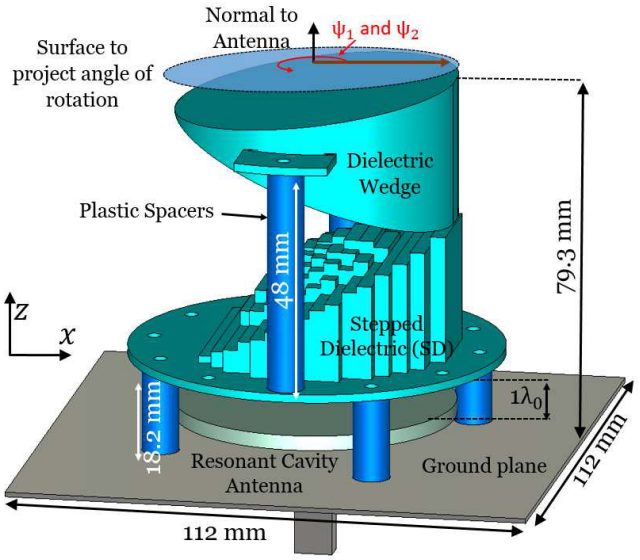

FIGURE 17. 3D model of the complete antenna system used in full-wave simulations.

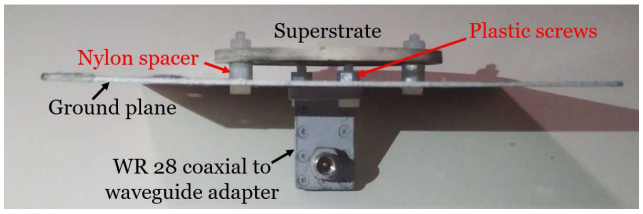

FIGURE 18. A photograph of the assembled RCA where WR-28 coaxial to waveguide adapter shown at the bottom has 2.92 SMA connector.

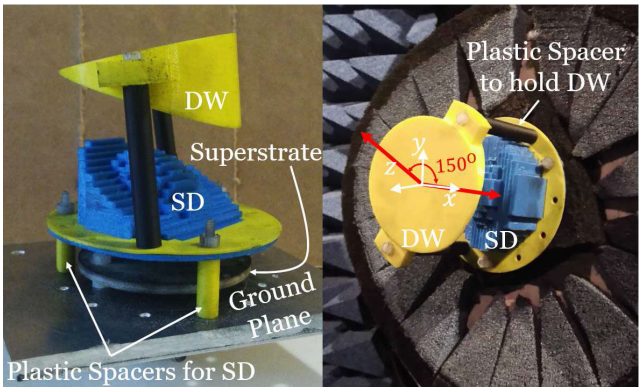

FIGURE 19. A picture of the fabricated and assembled prototype (left). Picture of the complete system fixed on the measurement stage in the anechoic chamber (right). For the sake of clarity, the absorber ring around the antenna has been removed. The two red arrows indicate the orientation of the SD and DW in the xy-plane.

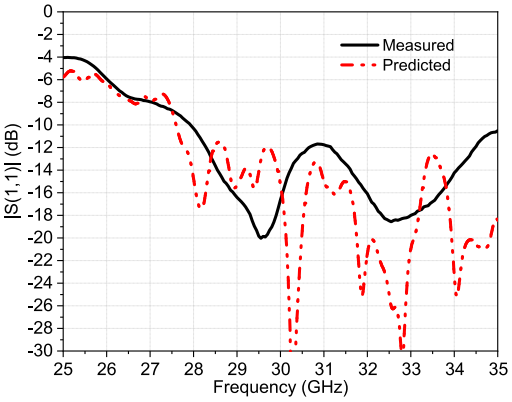

FIGURE 20. Comparison of measured and predicted magnitude of reflection coefficient in a frequency band around the operating frequency.

TABLE 1. Symbol used to explain the SD and DW rotation.

Parameter	Explanation	Value
ψ_1	Orientation SD	Changed dynamically
ψ_2	Orientation DW	Changed dynamically
ϕ	Azimuth angle of the beam peak	Dynamically controlled by ψ_1 and ψ_2
θ	Elevation angle of the beam peak	Dynamically controlled by ψ_1,ψ_2

DW are fabricated with a locally available 3D printer from Omni3D. The SD and DW were 3D printed with Polylactic acid (PLA). Two photographs of the developed prototype are shown in Fig. 19. In the first photograph on the left, the complete antenna system is shown. In the second photograph on the right, the prototype is fitted inside the anechoic chamber where feed is not visible. A ring of an RF absorber used around the antenna system to absorb lateral propagation and leakage of the electric field from the sides of the antenna system is not shown in these pictures.

The antenna was measured for impedance matching using a vector network analyzer (VNA). The magnitude of the reflection coefficient is less than -10 dB in a considerable band around the operating frequency, as shown in Fig. 20. For reference, the magnitude of the reflection coefficient predicted through simulations is also included in the figure. The direction of the antenna beam, represented in spherical coordinates θ and ϕ, is dynamically changed by physically rotating the SD and DW or changing ψ_1 and ψ_2 as summarized in Table 1. In the measurements, the SD is kept stationary or $\psi_1 = 0$ while the DW is rotated anticlockwise with a step of 30°. As the DW is rotated anticlockwise around the center of the aperture, the beam peak moves from the farthest point on the elevation plane towards the broadside direction. The movement of the beam peak follows a spiral pattern and both azimuth and elevation angles of the beam peak change. The movement is similar to that achieved by beam-steering antenna using near-field time-delay metasurfaces and graded-dielectric plates [12], [32]. For each orientation com-

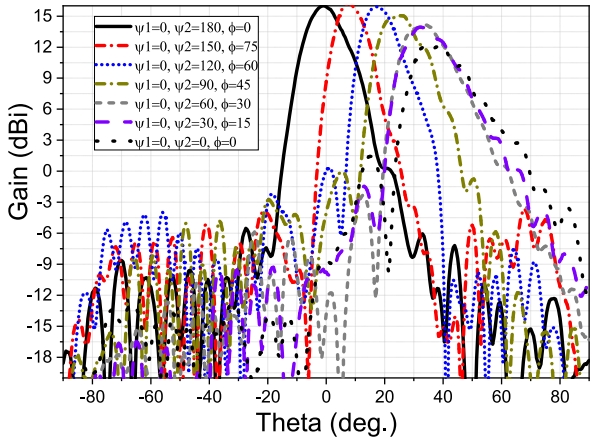

FIGURE 21. Far-field pattern elevation cuts, demonstrating beam scanning at the operating frequency of 30 GHz. Each pattern is taken at a different azimuth angle (ϕ) and for a specific rotation combination of the SW and DW (ψ_1 and ψ_2).

TABLE 2. Direction of antenna beam peak with the physical rotation of the DW.

ψ_1 (deg.)	ψ_2 (deg.)	Beam Peak (dBi)	ϕ (deg.)	θ (deg.)
0	0	12.2	0	39
0	30	13.9	15	32
0	60	14.1	30	34
0	90	15.1	45	25.5
0	120	15.9	60	17
0	150	16.2	75	7.5
0	180	16.0	0	1

bination of the SD and DW, the elevation pattern cuts are taken at azimuth angles containing the beam peak, which is given in Fig. 21. The direction of beam peaks and gain in the direction of beam peaks are summarized in Table 2.

The maximum peak gain of the antenna is 16.2 dBi, which occurs when the DW is rotated by 150° and the beam peak is closer to the broadside direction. The 3dB beamwidth of the antenna beam in the elevation cut is between 3° and 13.5° elevation angles, and thus have a 3dB beamwidth of the 9.5°. The minimum gain of the antenna is 12.2 dBi and the direction of the beam peak is at an elevation angle of 39°. The peak gain is 14.1 dBi at the elevation angle of 34° but drops sharply to 12.2 dBi when the peak is at the elevation angle of 39°. It can therefore be concluded that the antenna beam can be scanned to the maximum elevation angle of 34° while maintaining beam peak within 3dB of the maximum gain value of 16.2 dBi. Although the azimuth angle is also changing as given in Table 2, it is possible to scan the beam to any desired azimuth angle by co-rotating the SD and the DW, similar to the co-rotation of the graded dielectrics demonstrated reported in [32]. The co-rotation can be used to scan the antenna beam, whilst maintaining peak gain within −3 dB of maximum gain value, in an apex angle of 68° (2 × 34°). The co-rotation of the SD and DW is not verified through measurement because of the limited available time at the measurement facility.

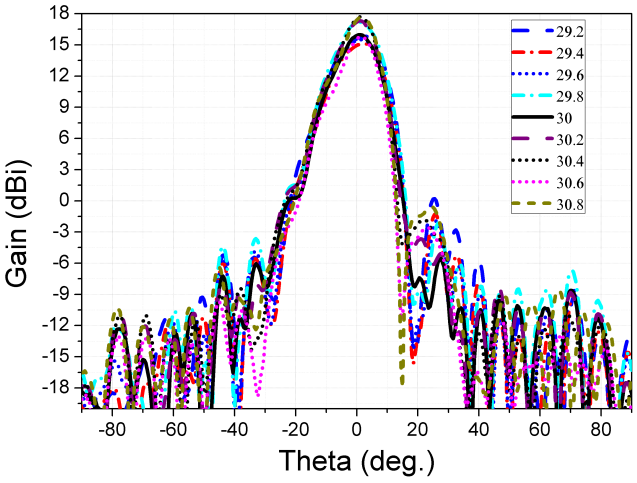

FIGURE 22. Far-field pattern cuts in a band around the center operating frequency taken at azimuth angle of $\phi = 0°$ for fixed orientations of SD and DW.

The antenna system has similar radiation performance in the 1.6 GHz frequency band measured around the center operating frequency of 30 GHz. The radiation patterns cuts of the antenna in a wider frequency band when the beam peak is in the broadside direction are plotted in Fig. 22.

The antenna was designed to operate at 30 GHz but for the case when the beam is in the broadside direction, the maximum gain was achieved at 30.4 GHz. To observe the beam-scanning performance of the antenna system at this frequency, the elevation pattern cuts of the far-field patterns taken by rotating the DW – as discussed above – are compared in Fig. 23. Almost identical performance, in terms of beam-peak pointing angle, is achieved at the two frequencies, which is encouraging because a beam-scanning antenna must be capable of maintaining beam in a fixed direction for different frequency channels. The peak gain, however, at the operating frequency was about 2 dB less than at 30.4 GHz. The shift in frequency is a typical phenomenon, which has been observed with the near-field phase transforming type structures [20]. The measured patterns in terms of shape and beam-peak angles are very close to those predicted by full-wave simulations. As a reference, predicted pattern cuts at the frequency of 30.4 GHz for five different orientations of DW are compared with the measured pattern cuts in Fig. 24. A slight shift in beam peaks in the measured patterns with respect to those predicted from simulations can be attributed to an error in the alignment of the antenna in the measurement facility.

The proposed antenna, because of the extremely low-cost and use of readily available basic 3D printers, can be developed without using a delicate manufacturing facility. The manufacturing cost of the SD and DW is less than 10 USD, which is calculated based on the weight of the material used in the printed dielectric structures. In contrast, the pair of metasurfaces using three printed layers costs more than 1500 USD [12]. The graded-dielectric plates based prototype may have comparable costs in the future, considering the rapid

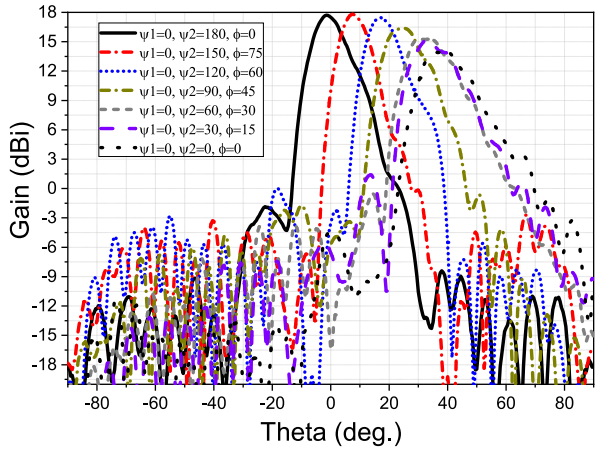

FIGURE 23. Far-field pattern cuts at the frequency of 30.4 GHz, taken in different elevation planes after rotating DW.

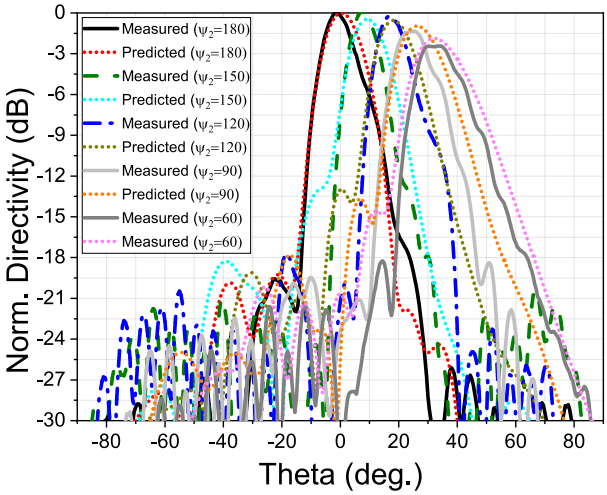

FIGURE 24. Comparison of predicted and measured patterns cuts taken at frequency 30.4 GHz. Patterns are taken when SD is fixed along x-axis (or $\psi_1 = 0$) and DW is rotated.

development taking place in the 3D printing materials. However, graded-dielectric plates are not practically feasible at this point in time.

The proposed beam-scanning antenna can be used in a range of low-cost applications or those requiring a larger number of transmit-receive terminal antennas. Apart from the ground stations, the antenna system can be used with CubeSat to establish satellite-to-satellite communication links. The antenna system can be used to develop a network of passive remote sensing base stations, which can be erected time efficiently and at an extremely low-cost. The parts required for these antenna systems can be 3D printed without any sophisticated machining or binding as required in all other traditional beam-steering antenna systems.

VI. CONCLUSION

An extremely low-cost beam-scanning antenna is developed using a pair of 3D printed stepped dielectric (SD) and dielectric wedge (DW) made from Polylactic acid (PLA). The total cost in printing the two dielectric structures is less than 10 USD. The SD and DW have been designed using the physics of near-field phase transformation and theory of electromagnetic (EM) wave propagation thorough a dielectric prism. The measurement results of the fabricated prototype indicate that by physically rotating the DW, it is possible to scan the antenna beam peak from the broadside direction to a maximum elevation angle of 39°. The combination of innovative design strategy and manufacturing technique yields an antenna system that can be deployed in large numbers to build necessary ground infrastructure for increasing the uplink and downlink connectivity time for CubeSat constellations.

REFERENCES

[1] J. Warshowsky, C. Kulisan, and D. Vail, "20 GHz phased array antenna for GEO satellite communications," in *Proc. 21st Century Mil. Commun. Archit. Technol. Inf. Superiority*, vol. 2, 2000, pp. 1187–1191.

[2] R. J. Mailloux, "Phased array theory and technology," *Proc. IEEE*, vol. 70, no. 3, pp. 246–291, Mar. 1982.

[3] B. Forman, "Directivity characteristics of scannable planar arrays," *IEEE Trans. Antennas Propag.*, vol. 20, no. 3, pp. 245–252, May 1972.

[4] B. Aragon, R. Houborg, K. Tu, J. B. Fisher, and M. McCabe, "CubeSats enable high spatiotemporal retrievals of crop-water use for precision agriculture," *Remote Sens.*, vol. 10, no. 12, p. 1867, Nov. 2018.

[5] K. Zhang and A. J. Gasiewski, "Microwave CubeSat fleet simulation for hydrometric tracking in severe weather," in *Proc. IEEE Int. Geosci. Remote Sens. Symp. (IGARSS)*, Jul. 2016, pp. 5569–5572.

[6] C. Surussavadee, W. J. Blackwell, D. Entekhabi, and R. V. Leslie, "Precipitation retrieval accuracies of the tropics constellation of passive microwave cubesats," in *Proc. IEEE Int. Geosci. Remote Sens. Symp. (IGARSS)*, Jul. 2018, pp. 3868–3871.

[7] B. Altena and A. Kääb, "Glacier ice loss monitored through the planet cubesat constellation," in *Proc. 9th Int. Workshop Anal. Multitemporal Remote Sens. Images (MultiTemp)*, Jun. 2017, pp. 1–4.

[8] W. J. Blackwell, "The MicroMAS and MiRaTA CubeSat atmospheric profiling missions," in *IEEE MTT-S Int. Microw. Symp.*, May 2015, pp. 1–3.

[9] Z. Zhang, G. Xu, and J. Song, "Cubesat cloud detection based on JPEG2000 compression and deep learning," *Adv. Mech. Eng.*, vol. 10, no. 10, 2018, Art. no. 1687814018808178, doi: 10.1177/1687814018808178.

[10] O. Popescu, "Power budgets for cubesat radios to support ground communications and inter-satellite links," *IEEE Access*, vol. 5, pp. 12618–12625, 2017.

[11] K. Dabrowska and M. Stolarski, "Ground segment of distributed ground station system," in *Proc. Int. Conf. Comput. Tool (EUROCON)*, Sep. 2007, pp. 894–900.

[12] M. U. Afzal and K. P. Esselle, "Steering the beam of medium-to-high gain antennas using near-field phase transformation," *IEEE Trans. Antennas Propag.*, vol. 65, no. 4, pp. 1680–1690, Apr. 2017.

[13] L. Zhou, X. Chen, X. Duan, and J. Li, "FPA using a three-layer PSS for gain enhancement," *IET Microw., Antennas Propag.*, vol. 12, no. 3, pp. 400–405, Feb. 2018.

[14] M. Sun, Nasimuddin, X. Qing, and Z. N. Chen, "Circularly polarized switched beams grid array antenna for mm-wave systems," in *Proc. IEEE Asia–Pacific Microw. Conf. (APMC)*, Dec. 2019, pp. 1598–1600.

[15] A. Barison, P. Deo, and D. Mirshekar-Syahkal, "A switched beam 60 GHz 2×2-element planar antenna array," in *Proc. 8th Eur. Conf. Antennas Propag. (EuCAP)*, Apr. 2014, pp. 1000–1002.

[16] C. D. McEwen and M. R. Khan, "Beam steering method with improved sidelobe response using dielectric wedges for satellite TV reception," in *Proc. 14th Eur. Microw. Conf.*, Sep. 1984, pp. 681–685.

[17] H. D. Griffiths and M. R. Khan, "Antenna beam steering technique using dielectric wedges," *IEE Proc. H Microw., Antennas Propag.*, vol. 136, no. 2, pp. 126–131, Apr. 1989.

[18] N. Gagnon and A. Petosa, "Using rotatable planar phase shifting surfaces to steer a high-gain beam," *IEEE Trans. Antennas Propag.*, vol. 61, no. 6, pp. 3086–3092, Jun. 2013.

[19] A. A. Baba, R. M. Hashmi, K. P. Esselle, M. Attygalle, and D. Borg, "A millimeter-wave antenna system for wideband 2-D beam steering," *IEEE Trans. Antennas Propag.*, vol. 68, no. 5, pp. 3453–3464, May 2020.
[20] M. U. Afzal, K. P. Esselle, and B. A. Zeb, "Dielectric phase-correcting structures for electromagnetic band gap resonator antennas," *IEEE Trans. Antennas Propag.*, vol. 63, no. 8, pp. 3390–3399, Aug. 2015.
[21] M. Akbari, M. Farahani, A. Ghayekhloo, S. Zarbakhsh, A.-R. Sebak, and T. A. Denidni, "Phase gradient surface approaches for 60 ghz beam tilting antenna," *IEEE Trans. Antennas Propag.*, vol. 68, no. 6, pp. 4372–4385, Jun. 2020.
[22] Y. Lu, Y. Zhou, M. Hei, and D. Fan, "Theoretical and experimental determination of steering mechanism for Risley prism systems," *Appl. Opt.*, vol. 52, no. 7, pp. 1389–1398, 2013. [Online]. Available: http://ao.osa.org/abstract.cfm?URI=ao-52-7-1389
[23] S. J. Orfanidis, "Reflection and transmission," in *Electromagnetic Waves and Antennas*. Piscataway, NJ, USA: Rutgers Univ., 2008.
[24] G. V. Trentini, "Partially reflecting sheet arrays," *IRE Trans. Antennas Propag.*, vol. 4, no. 4, pp. 666–671, Oct. 1956.
[25] A. R. Weily, K. P. Esselle, B. C. Sanders, and T. S. Bird, "High-gain 1D EBG resonator antenna," *Microw. Opt. Technol. Lett.*, vol. 47, no. 2, pp. 107–114, 2005, doi: 10.1002/mop.21095.
[26] H. Yang and N. Alexopoulos, "Gain enhancement methods for printed circuit antennas through multiple superstrates," *IEEE Trans. Antennas Propag.*, vol. 35, no. 7, pp. 860–863, Jul. 1987.
[27] Y. Vardaxoglou and F. Capolino, "Review of highly-directive flat-plate antenna technology with metasurfaces and metamaterials," in *Proc. 36th Eur. Microw. Conf.*, Sep. 2006, pp. 963–966.
[28] M. U. Afzal, K. P. Esselle, and A. Lalbakhsh, "A methodology to design a low-profile composite-dielectric phase-correcting structure," *IEEE Antennas Wireless Propag. Lett.*, vol. 17, no. 7, pp. 1223–1227, Jul. 2018.
[29] A. Hosseini, A. T. Almutawa, F. Capolino, and D. R. Jackson, "Wideband single-layer Fabry-Pérot cavity antenna with a radial variation of the cavity permittivity," in *Proc. IEEE Int. Symp. Antennas Propag. USNC/URSI Nat. Radio Sci. Meeting*, Jul. 2017, pp. 2659–2660.
[30] K. Cao, F. Xu, and L. Yang, "Low-profile dual-band Fabry–Pérot resonator antenna," in *Proc. 6th Asia–Pacific Conf. Antennas Propag. (APCAP)*, Oct. 2017, pp. 1–3.
[31] *CWR28KD 2.92/Female to WR28 Coaxial to Waveguide Adapter 26.5-40 GHZ, Rev. 000.*, Centric RF, Allen, TX, USA, 2019.
[32] M. U. Afzal, A. Lalbakhsh, and K. P. Esselle, "Electromagnetic-wave beam-scanning antenna using near-field rotatable graded-dielectric plates," *J. Appl. Phys.*, vol. 124, no. 23, Dec. 2018, Art. no. 234901.

MUHAMMAD U. AFZAL (Senior Member, IEEE) received the bachelor's degree (Hons.) in electronics engineering and the master's degree in computational science and engineering from the National University of Sciences and Technology (NUST), Islamabad, Pakistan, in 2005 and 2011, respectively, and the Ph.D. degree from Macquarie University, Sydney, NSW, Australia, in 2017.

He was a Laboratory Engineer with the Samar Mubarakmand Research Institute of Microwave and Millimeterwave Studies (SMRIMMS), Islamabad, from 2010 to 2012. He was also a Lecturer with the Electrical Engineering Department, NUST, from 2012 to 2013. He has developed the concept of near-field phase correction to enhance the directivity of low-gain aperture antennas with the IEEE TAP Paper entitled Dielectric Phase-Correcting Structures for Electromagnetic Band-Gap Resonator Antennas. He is a co-inventor of efficient antenna beam-steering technology that developed using near-field metasurfaces. He also led a team of colleagues in CSIRO sponsored ON Prime Two in 2017–Pre-Accelerator Program designed to commercialise outcomes of academic research. His research interests include development of electromagnetic phase-shifting structures, frequency selective surfaces, and similar metamaterials for microwave and millimetre-wave antenna applications. He received the Highly Commended Certificate in Five Future-Shaping Research Priorities category from the 2017 Academic Staff Awards. He received several awards and scholarships, including the Merit-Based Scholarship in six out of eight semesters during undergraduate, a scholarship of complete fee waiver during the postgraduate studies, and an International Macquarie Research Excellence (iMQRES) Scholarship towards the Doctorate study from Macquarie University. He also received the Competitive Travel Grant to research work from the Flagship Conference through the Antennas and Propagation Society (APS), Vancouver, BC, Canada, in 2015.

LADISLAU MATEKOVITS (Senior Member, IEEE) received the degree in electronic engineering from the Institutul Politehnic din Bucureşti, Bucureşti, Romania, in 1992, and the Ph.D. degree (Dottorato di Ricerca) in electronic engineering from the Politecnico di Torino, Torino, Italy, in 1995.

Since 1995, he has been with the Department of Electronics and Telecommunications, Politecnico di Torino, as a Postdoctoral Fellowship and a Research Assistant. He joined the Department of Electronics and Telecommunications as an Assistant Professor, in 2002, a Senior Assistant Professor, in 2005, and an Associate Professor, in 2014. In 2005, he was a Visiting Scientist with the Antennas and Scattering Department, FGAN-FHR (Fraunhofer Institute), Wachtberg, Germany. In July 2009, he was a Marie Curie Fellow with Macquarie University, Sydney, NSW, Australia, for a period of two years, where he also held a Visiting Academic position, in 2013. In 2014, he was an Honorary Fellow. In February 2017, he was a Full Professor national qualification, Italy. Since 2020, he has been an Honorary Professor with the Polytechnic University of Timisoara. He held an Associate position with the Italian National Research Council. His main research interests include numerical analysis of printed antennas and in particular development of new, numerically efficient full-wave techniques to analyze large arrays, active and passive metamaterials for various applications as cloaking, non-radiating (anapole) modes and/or topological states, DRA, and graphen-based antennas. Material parameter retrieval of these structures by inverse methods and different optimization techniques has also been considered. Bio-electromagnetic aspect has been contemplated, as a design of implantable antennas or development of nano-antennas for example a drug delivery applications. He has published more than 360 articles, including over 80 journal contributions, and delivered seminars on these topics all around the world, such as Europe, USA (AFRL/MIT-Boston), Australia, China, and Russia. He was invited to serve as a Research Grant Assessor for government funding calls in Romania, Italy, and Croatia, and an International Expert in the Ph.D. thesis evaluation by several Universities with Australia, India, Pakistan, Spain, and so on.

Dr. Matekovits was a member of the National Council for the Attestation of University Degrees, Diplomas, and Certificates (CNATDCU), Romania. Since 2010, he has been a member of the Organizing Committee with the International Conference on Electromagnetics in Advanced Applications (ICEAA). He is also a member of the technical program committees of several conferences. He has been an Assistant Chairman and the Publication Chairman with the European Microwave Week, Milan, Italy, in 2002, and the General Chair of the 11th International Conference on Body Area Networks (BodyNets), in 2016. He was a recipient of various awards in international conferences, including the 1998 URSI Young Scientist Award, Thessaloniki, Greece, the Barzilai Award in 1998 (Young Scientist Award granted every two years by the Italian National Electromagnetic Group), the Best AP2000 Oral Paper on Antennas, and the ESA-EUREL Millennium Conference on Antennas and Propagation, Davos, Switzerland. He was also a recipient of the Motohisa Kanda Award for the most cited article from the IEEE TRANSACTIONS ON ELECTROMAGNETIC COMPATIBILITY in 2019. He serves as an Associate Editor for IEEE ACCESS, the IEEE ANTENNAS AND WIRELESS PROPAGATION LETTERS, and *IET MAP*. He also serves as a Reviewer for different journals.

KARU P. ESSELLE (Fellow, IEEE) is the Distinguished Professor in Electromagnetic and Antenna Engineering at the University of Technology Sydney and a Visiting Professor of Macquarie University, Sydney. According to a Special Report on Research published by The Australian national newspaper in 2019, he is the National Research Field Leader in Australia in Microelectronics in Engineering Discipline as well as in the Electromagnetism field in the Disciplines of Physics and Mathematics.

Karu received BSc degree in electronic and telecommunication engineering with First Class Honours from the University of Moratuwa, Sri Lanka, and MASc and PhD degrees with near-perfect GPA in electrical engineering from the University of Ottawa, Canada. Previously he was Director of WiMed Research Centre and Associate Dean - Higher Degree Research (HDR) of the Division of Information and Communication Sciences and directed the Centre for Collaboration in Electromagnetic and Antenna Engineering at Macquarie University. He has also served as a member of the Dean's Advisory Council and the Division Executive and as the Head of the Department several times. Karu is a Fellow of IEEE, the Royal Society of New South Wales and Engineers Australia.

Since 2018, Karu has been chairing the prestigious Distinguished Lecturer Program Committee of the IEEE Antennas and Propagation (AP) Society - the premier global learned society dedicated for antennas and propagation - which has close to 10,000 members worldwide. After two stages in the selection process, Karu was also selected by this Society as one of two candidates in the ballot for 2019 President of the Society. Only three people from Asia or Pacific apparently have received this honour in the 68-year history of this Society. Karu is also one of the three Distinguished Lecturers (DL) selected by the Society in 2016. He is the only Australian to chair the AP DL Program ever, the only Australian AP DL in almost two decades, and second Australian AP DL ever (after UTS Distinguished Visiting Professor Trevor Bird). He has been continuously serving the IEEE AP Society Administrative Committee in several elected or ex-officio positions since 2015. Karu is also the Chair of the Board of management of Australian Antenna Measurement Facility, and was the elected Chair of both IEEE New South Wales (NSW), and IEEE NSW AP/MTT Chapter, in 2016 and 2017.

Karu has authored approximately 600 research publications and his papers have been cited over 10,000 times. In 2019 his publications received 1,200 citations. He is the first Australian antenna researcher ever to reach Google Scholar h-index of 30 and his citation indices have been among the top Australian antenna researchers for a long time (at present: i10 is 180 and h-index is 49). Since 2002, his research team has been involved with research grants, contracts and PhD scholarships worth about 20 million dollars, including 15 Australian Research Council grants, without counting the 245 million-dollar SmartSat Corporative Research Centre, which started in 2019. His research has been supported by many national and international organisations including Australian Research Council, Intel, US Air Force, Cisco Systems, Hewlett-Packard, Australian Department of Defence, Australian Department of industry, and German and Indian governments.

Karu's awards include one of the two finalists for 2020 Australian Eureka Prize for Outstanding Mentor of Young Researchers, 2019 Motohisa Kanda Award (from IEEE USA) for the most cited paper in IEEE Transactions on EMC in the past five years, 2019 Macquarie University Research Excellence Award for Innovative Technologies, 2019 ARC Discovery International Award, 2017 Excellence in Research Award from the Faculty of Science and Engineering, 2017 Engineering Excellence Award for Best Innovation, 2017 Highly Commended Research Excellence Award from Macquarie University, 2017 Certificate of Recognition from IEEE Region 10, 2016 and 2012 Engineering Excellence Awards for Best Published Paper from IESL NSW Chapter, 2011 Outstanding Branch Counsellor Award from IEEE headquarters (USA), 2009 Vice Chancellor's Award for Excellence in Higher Degree Research Supervision and 2004 Innovation Award for best invention disclosure. His mentees have been awarded many fellowships, awards and prizes for their research achievements. Fifty international experts who examined the theses of his PhD graduates ranked them in the top 5

Karu has provided expert assistance to more than a dozen companies including Intel, Hewlett Packard Laboratory (USA), Cisco Systems (USA), Audacy (USA), Cochlear, Optus, ResMed and Katherine-Werke (Germany). His team designed the high-gain antenna system for the world's first entirely Ka-band CubeSat made by Audacy, USA and launched to space by SpaceX in December 2018. This is believed to be the first Australian-designed high-gain antenna system launched to space, since CSIRO-designed antennas in Australia's own FedSat launched in 2002.

Karu is in the College of Expert Reviewers of the European Science Foundation (2019-22) and he has been invited to serve as an international expert/research grant assessor by several other research funding bodies as well, including the European Research Council and funding agencies in Norway, Belgium, the Netherlands, Canada, Finland, Hong-Kong, Georgia, South Africa and Chile. He has been invited by Vice-Chancellors of Australian and overseas universities to assess applications for promotion to professorial levels. He has also been invited to assess grant applications submitted to Australia's most prestigious schemes such as Australian Federation Fellowships and Australian Laureate Fellowships. In addition to the large number of invited conference speeches he has given, he has been an invited plenary/extended/keynote speaker of several IEEE and other conferences and workshops including EuCAP 2020 Copenhagen, Denmark; URSI'19 Seville, Spain; and 23rd ICECOM 2019, Dubrovnik, Croatia.

He is an Associate Editor of IEEE Transactions on Antennas Propagation, IEEE Antennas and Propagation Magazine and IEEE Access. He is a Track Chair pf IEEE AP-S 2020 Montreal, Technical Program Committee Co-Chair of ISAP 2015, APMC 2011 and TENCON 2013 and the Publicity Chair of ICEAA/IEEE APWC 2016, IWAT 2014 and APMC 2000. His research activities are posted in the web at http://web.science.mq.edu.au/∼esselle/ and https://www.uts.edu.au/staff/karu.esselle.

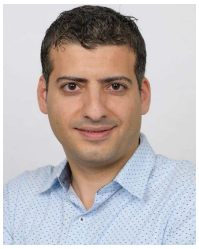

ALI LALBAKHSH (Member, IEEE) received the B.S. and M.S. degrees in electronic and telecommunication engineering from Islamic Azad University, Iran, in 2008 and 2011, respectively, and the Master of Research (H.D.) and Ph.D. degrees in electronics engineering from Macquarie University, Australia, in 2015 and 2020, respectively. He holds a Sessional Academic position with the Macquarie University. He has authored or coauthored around 60 peer-reviewed journal and conference papers. His research interests include resonance-based antennas, frequency selective surfaces, electromagnetic metasurfaces, periodic and electromagnetic band gap structures, evolutionary optimisation methods, and microwave passive components. He received several prestigious awards, including the International Research Training Program Scholarship (iRTP) for the MRes, the International Macquarie University Research Excellence Scholarship (iMQRES) for the Ph.D. degree, the Commonwealth Scientific and Industrial Research Organization (CSIRO) grants on Astronomy and Space Exploration, the Macquarie University Postgraduate Research Fund (PGRF), and the WiMed Travel Support Grants. He was a recipient of the 2016 ICEAA-IEEE APWC Cash Prize and the Macquarie University Deputy Vice-Chancellor Commendation in 2017. He is the only Researcher with the IEEE Region Ten (Asia-Pacific) who received the Most Prestigious Best Paper Contest of the IEEE Region Ten more than once. He was awarded Third Prize in 2016, First Prize in 2018, and Second Prize in 2019 from the International Competition. He was nominated for the 2019 Excellence in Higher Degree Research Award-Science, Technology, Engineering, Mathematics and Medicine (STEMM), Macquarie University. He serves as an Associate Editor for the *AEÜ-International Journal of Electronics and Communications*.